Glucose sensing by absorption spectroscopy using lensed optical fibers

SILJE S. FUGLERUD,[1,2,*] KAROLINA B. MILENKO,[1] REINOLD ELLINGSEN,[1] ASTRID AKSNES,[1] AND DAG R. HJELME [1]

[1] *Department of Electronic Systems, Norwegian University of Science and Technology, Trondheim NO-7491, Norway*
[2] *St. Olavs University Hospital, Trondheim NO-7030, Norway*
[*] *silje.fuglerud@ntnu.no*

Abstract: The bulkiness of common transmission spectroscopy probes prevents applicability at remote locations such as within the body. We present the fabrication and characterization of lensed fibers for transmission spectroscopy in the near infrared. Eigenmode simulations and measurements of the coupling efficiency are presented and applied to design the setup corresponding to the sample absorption. Sensing capabilities are demonstrated on aqueous glucose samples ranged 80 to 500 mM obtaining a mean absolute percentage error of calibration of 4.3 %. With increased flexibility, transmission spectroscopic sensors at remote locations may be achievable, for example applied to *in vivo* continuous glucose monitoring.

1. Introduction

Diabetes mellitus is a disease affecting 422 million people in 2014 [1], corresponding to 7.9 to 9 % of the world's population. A subset of these patients with diabetes mellitus type 1 require tight control of their blood glucose to avoid harmful effects of either too high (hyperglycemia) or too low (hypoglycemia) blood sugar levels. The state-of-the-art treatment are continuous subcutaneous electrochemical sensors that measure in the interstitial fluid, giving the patients a higher level of glycemic control. However, these sensors must be replaced frequently, require frequent calibration and the glucose concentration in the interstitial fluid is delayed 10 to 15 min compared to the blood glucose level. As an alternative, spectroscopy-based optical glucose sensing have been suggested to provide a long-term option for continuous glucose measurements [2, 3]. Due to the lack of chemical reagents that can degrade in spectroscopy-based sensors, it is reasonable to expect less frequent exchange and calibration of such a sensor than the current electrochemical sensors. Several research groups have shown that accurate glucose sensing from the near infrared (NIR) absorption spectrum is possible [4], and that other biological molecules can be measured simultaneously by utilizing multivariate calibration. A popular research topic has been non-invasive NIR glucose measurements [3, 5], but the technique has not yet been successfully commercialized due to difficulties in calibration on the skin across different patients. By measuring directly in a bodily fluid this problem can be avoided. Previous NIR absorption spectroscopy studies have measured bodily fluids *in vitro* [6], indicating that the technique can be applied *in vivo* with a suitable probe. A viable candidate is the peritoneal fluid, a water-like fluid where the glucose dynamics appear to be faster [7] than the interstitial fluid and the immunological reaction is not as severe as in blood. In this paper, we present a fiber-based transmission probe created for the future application of spectroscopic measurements in the peritoneal fluid *in vivo*. By utilizing a broad wavelength range, several spectral features of glucose can be measured simultaneously, enabling enough channels to account for interfering molecules yielding a label-free, glucose specific sensor.

Fibers are advantageous as a light guide as they can deliver light to remote locations, for example into the body. Compared to common integrated spectrometers, having the source and

detector separate provides a higher level of flexibility. In collimated light spectrometers, the measurement chamber must be shielded to avoid light leaking into the system. In the setup presented here, the limited numerical aperture (NA) of the lenses grant only collection of beams with a small entrance angle, which minimizes the influence of stray light entering the detector. Coupling light into and out of fibers separated by a distance as required in transmission spectroscopy usually involves bulk optics, and has therefore not been small enough for *in vivo* applications even when miniaturized [8] ($5 \times 8 \times 5$ mm). In order to avoid bulk optics altogether, the interaction region is here created between two fibers with focusing lenses on the fiber facets as shown in Fig. 1. Such lenses can be easily manufactured [9, 10]. The benefits and use of lensed fibers for imaging and sensing applications has previously been applied to optical coherence tomography [11], optical trapping [12] and fluorescence spectroscopy [13, 14], mainly for depth resolved applications. Looch [15] used lensed fibers in a fiber loop cavity ring down absorption spectroscopy setup. On the topic of lensed fibers applied to glucose sensing, a somewhat similar reflectance probe [16] made from a ball lens and a large core optical fiber has been used in a non-invasive rat study. A ball-lens sensor based on a single mode (SM) fiber with a mirror has also been applied *in vitro* to aqueous glucose [17], but only using the peak power corresponding to one wavelength channel. Beyond these studies, lensed fibers do not appear well explored for monitoring or sensing of aqueous samples such as glucose by NIR spectroscopy.

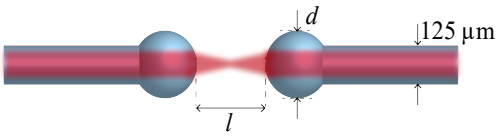

Fig. 1: The proposed setup for transmission spectroscopy, with variable path length l and micro-lens sphere size d.

NIR spectroscopy in water solutions poses a challenge with balancing the optical path length l and the water absorption. A certain interaction length is needed for an acceptable signal, requiring a minimum path length. For solutions in water, the strong absorption results in a very low signal at certain wavelengths. This places a constraint on the upper limit of the path length. Herein, we demonstrate how to select the sphere size d of the lenses such that the insertion loss is minimized at the optimum path length l matched to the wavelength range of interest. We have limited the analysis to lenses that can be created directly on the fiber tips and not to investigate smaller lenses that could be created by tapering and therefore give shorter focal lengths. After covering the governing formulas, we present the fabrication of such lenses on a multi mode (MM) fiber end facet, followed by eigenmode simulations of the focusing in water. Simulations are compared with experimentally determined coupling efficiencies. Finally, the spectrometer configuration is applied to a series of glucose solutions.

2. Theory

NIR vibrational spectroscopy makes use of the concentration dependent absorption of the sample constituents. At a given wavelength, the absorbance can be found from Beer's law

$$A = \sum_{i=1}^{N} (\epsilon_i c_i + \mu_i)\, l, \tag{1}$$

where N is the number of different constitutents in the sample (both the solvent and solutes), ϵ_i is the molar absorptivity of the i-th analyte at the given wavelength, c_i is the concentration of the i-th analyte and l is the path length the light has traveled through the sample. The scattering caused by the sample, μ_i, is considered to be an extra attenuation term [18] and

often neglected in comparison with the much stronger absorption. The absorption coefficient is defined as $\alpha = \sum_{i=1}^{N} \epsilon_i c_i$. In a solution with solutes where water is used as a solvent, a reduction in the concentration of water must be accounted for by a displacement factor f, so that $\alpha = \epsilon_{\text{sol}} c_{\text{sol}} + \epsilon_{H_2O}(c_{H2O} - f c_{\text{sol}})$, where c_{sol} is the concentration of the solute and ϵ_{sol} is the molar absorptivity of the solute. As a result of attenuation, the transmitted intensity is

$$I(l, \lambda) = I_0(\lambda) \exp[-A(\lambda, l)], \tag{2}$$

where I_0 is the reference intensity. A reference intensity measurement is taken without a sample in the beam. Experimentally, the absorbance at a given wavelength can be determined from the relation

$$A = -\ln\left(\frac{I}{I_0}\right). \tag{3}$$

Here, the wavelength region of interest is 1 µm to 2.4 µm based on known glucose absorption bands [19]. From absorption originating from particular molecular vibrations, the sub-regions are labeled the short wave band (1 to 1.5 µm), the first overtone (1.5 to 1.85 µm), and the combination band (2.1 to 2.4 µm). Strong water absorption dominates the region 1.85 µm to 2.1 µm. The water attenuation is weak in the short wave band, and more prominent in the combination band than in the first overtone.

The path length l and the wavelength dependent molar absorptivity ϵ_i will impact the signal to noise ratio (SNR). Jensen and Bak [18] investigated the optimal path length to achieve the highest SNR in aqueous samples. In essence, the optimal length is inversely proportional to the absorption. Due to the strong water absorption, the optimal path length in the combination band was found to be between 0.4 and 0.5 mm. In the first overtone, where the water absorption is lower, the optimal path length was 1 mm to 2 mm. In the short wave band, the optimal path length varies from 0.5 mm to several mm due to the low water absorption in part of this region.

In this paper, spherically shaped lenses are used to focus the light for optimum transmitted power. The output power can be expressed as

$$P_{\text{out}} = \kappa(l) P_{\text{in}} \exp[-A(\lambda, l)], \tag{4}$$

where P_{in} is the input power and $\kappa(l)$ is a coupling loss factor smaller than 1. The factor $\exp[-A(\lambda, l)]$ is the attenuation due to absorption, which supplies the solute-dependent signal. To achieve a high signal strength for a given path length l, the transmission system should be designed so that $\kappa(l) \to 1$. To this end, the lenses created on the fiber tips should be fashioned as a $2f$-system to match the path length. In order to calculate the lens properties of fiber lenses, the paraxial geometrical (ray) optics approximation has previously been used [20]. From the thick lens formula, the focal length simplifies to

$$f_{\text{lens}} = \frac{n_{\text{medium}} R}{n_{\text{L}} - n_{\text{medium}}}, \tag{5}$$

where f is the focal length, n_{L} and n_{medium} are the refractive indices of the material of the spherical lens and the outside medium, respectively, and R is the curvature of the lens [21]. For this special case, the principal plane coincides with the curvature of the lens and the working distance is equal to the focal length.

3. Lensed fiber fabrication

MM fibers with 0.22 NA and 105 µm core diameter from Thorlabs (USA) were lensed using an FSM-100P ARCMaster by Fujikura (Japan). The spherical lens at the fiber tip is created by melting both the core and the cladding of the fiber by an arc, while the fiber is rotated around its axis. This procedure counteracts the pull of gravity and leads to a uniform spherical fiber tip.

The resulting size of the spheres was measured in the ARCMaster. Due to the large core of the MM fiber, a beam expansion region as used in other single mode (SM) fiber applications [9, 11] is not necessary.

We were able to manufacture spheres of diameter from 135 µm to 350 µm. For larger spheres (~ 350 µm), scattering or back-reflection from the lens tip and back to the fiber was observed (see Fig. 2). The contribution of loss in the spheres appears to be smaller than the variance in quality of the cleave and is therefore not easily quantifiable.

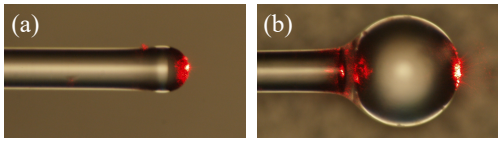

Fig. 2: Lensed fiber tips, sized (a) 150 µm and (b) 350 µm with red light propagating through.

4. Probe design for transmission spectroscopy

4.1. Focal length from eigenmode simulations

In order to determine the optimal lens diameter d in the design of the lenses, the properties of lensed fiber facets were investigated in two dimensions with the eigenmode expansion tool ModePROP by RSoft (Synopsys, USA). The optimal $\kappa(l)$ for a given $l = l_{\text{opt}}$ is assumed to occur for a $2f$-system. A Gaussian beam (beam diameter 125 µm) was launched in a fiber of diameter 125 µm with 105 µm core and 20 µm cladding. The core was pure silica ($n_{\text{core, 1.6 µm}} = 1.443$ and $n_{\text{core, 2.2 µm}} = 1.435$ [22]) and the NA was 0.22, resulting in a cladding refractive index of $n^2_{\text{clad}} = n^2_{\text{core}} - \text{NA}^2$. The launched light was propagated for 3.3 cm, corresponding to the Rayleigh length at $\lambda = 2.2$ µm. The exact distribution of the refractive index after lensing is unknown. Due to the high viscosity of silica and short arc bursts, a uniform mixing is unlikely. The final refractive index distribution is presumably a graded transition from core to cladding. As most of the fiber volume and therefore the lens end face is comprised of the core refractive index (71 %), the sphere was approximated to having the same refractive index as the core. Tabulated values of the refractive indices were adapted from the literature (silica glass [22] and water [23]). The simulations were performed at wavelengths 1.6 µm and 2.2 µm in air and water.

Fig. 3 and 4 show the predicted beam profiles of lensed fibers in water with absorption included. Overall, the focusing properties of the lensed fibers compares well with the geometrical optics approximation. Small diameter beams result in short focal length and a small spot size compared to large diameter lenses. However, the simulation demonstrates that the lensed fibers are unable to focus the higher order rays (modes). This will result in a reduced coupling coefficient for the $2f$ system in Fig. 1.

As expected, the attenuation due to water absorption (absorption coefficients $\alpha_{\lambda=1.6\,\mu\text{m}} = 6.7\,\text{cm}^{-1}$ and $\alpha_{\lambda=2.2\,\mu\text{m}} = 16.5\,\text{cm}^{-1}$ [24]) is more pronounced in the combination band than in the first overtone. To compare the simulations to the calculated focal length found using the geometrical optics approximation in Eq. (5), the maximum of the center cross-section of the beam profiles excluding absorption was found. The extracted focal lengths are plotted with the geometrical optics approximation in Fig. 5. Although the eigenmode simulations follow the lens formula in Eq. (5), they display a somewhat shorter focal length. The deviation from linear behavior with increasing sphere diameter is likely due to the finite number of modes excited in the MM fiber. Furthermore, we note that the observed focal length will depend on the exact mode excitation. The analysis illustrates that the excited modes in a MM fiber adds complexity compared to the geometrical optics approximation.

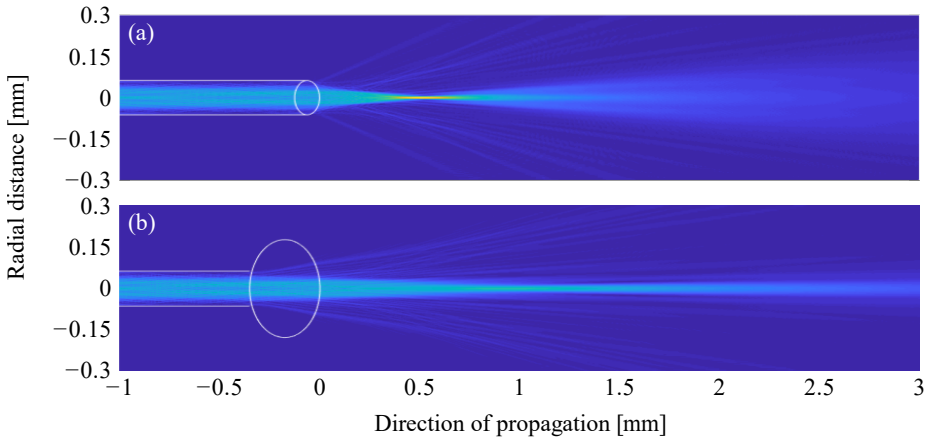

Fig. 3: Beam profile of spherical lensed fibers in water simulated for the first overtone (1.6 µm) using RSoft ModePROP. Absorption is included. In (a), a sphere with diameter 125 µm and in (b), a sphere with diameter 350 µm

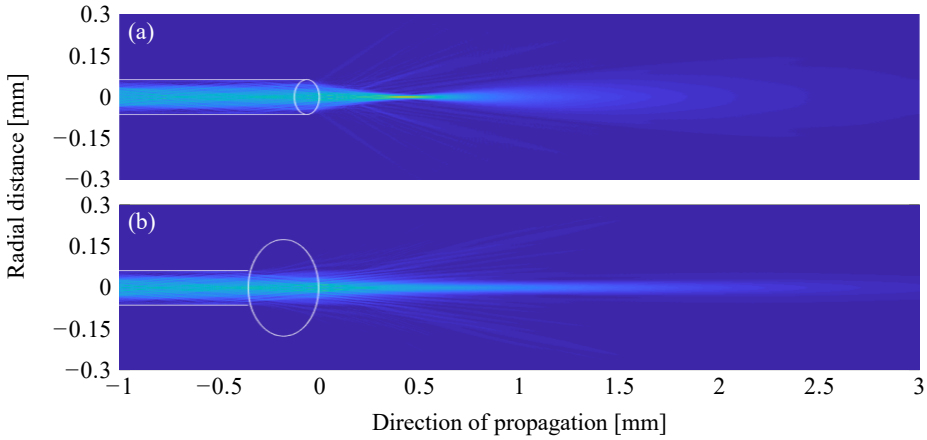

Fig. 4: Beam profile of spherical lensed fibers in water simulated for the combination band (2.2 µm) using RSoft ModePROP. Absorption is included. In (a), a sphere with diameter 125 µm and in (b), a sphere with diameter 350 µm.

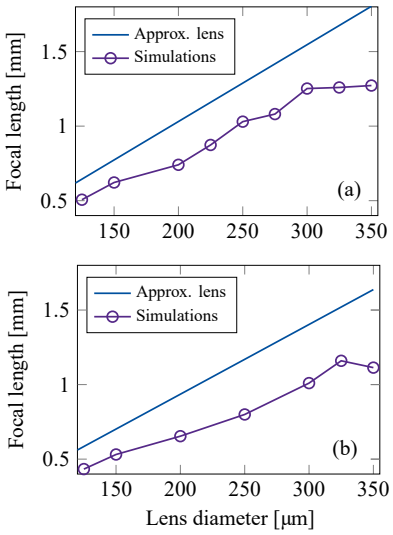

Fig. 5: The focal length of a lensed fiber tip in water using the geometrical optics approximation from Eq. (5) plotted with eigenmode simulations. (a) and (b) correspond to wavelengths 1.6 µm and 2.2 µm, respectively.

Optimal parameters	l	d
First overtone (1.6 µm)	1 to 2 mm	125 to 250 µm
Combination band (2.2 µm)	0.4 to 0.5 mm	125 µm

Table 1: The predicted optimal spherical lens diameter d at the optimal l in water (as presented by [18]) for the wavelength ranges of interest as a result of eigenmode simulations.

To summarize the eigenmode analysis, we list the design parameters that should be chosen for aqueous samples in Fig. 1 in Table 1. The optimum path lengths l are as presented by Jensen and Bak [18] and the sphere size d gives the $2f$-system for these path lengths. From Fig. 5(a), the matching spherical lens size range is 125 µm to 250 µm for the first overtone (l =1 to 2 mm). For measurements in the combination band, all the simulated lens diametres give a longer focal length than 0.25 mm (Fig. 5(b)). The smallest achievable lens created directly on the fiber tip without tapering is 125 µm in diameter. This would give the shortest focus and is therefore recommended for the combination band.

4.2. Experimental characterization

To arrive at the final design, the coupling efficiencies as a function of distance was investigated on the basis of the eigenmode analysis. An OceanOptics (USA) NIRQuest 512-2.5 spectrometer and a Thorlabs (USA) SL201L 10 mW broad band light source was connected to standard 0.22 NA MM fiber path cables (M15L01, SMA-FC/PC M100L01, Thorlabs). The fibers were fixed in v-grooves on xyz-translation stages (Thorlabs), aligned at l = 0 mm and pulled back with a µm-screw with an accuracy of ±5 µm. A dark noise spectrum was recorded at the beginning of every series.

For every sphere size, and for cleaved fibers, a measurement series was first taken in air. The curves are plotted for 150 µm, 200 µm and 350 µm spheres in Fig. 6(a). The transmittance is normalized to the maximum measured for each lens diameter. A higher power was measured at the sharp peak of the 150 µm lens than at the broader peak of the 350 µm lens. Broadening and

decreasing power of the peaks with increasing sphere size display a similar trend as the intensity profiles obtained from the eigenmode simulations.

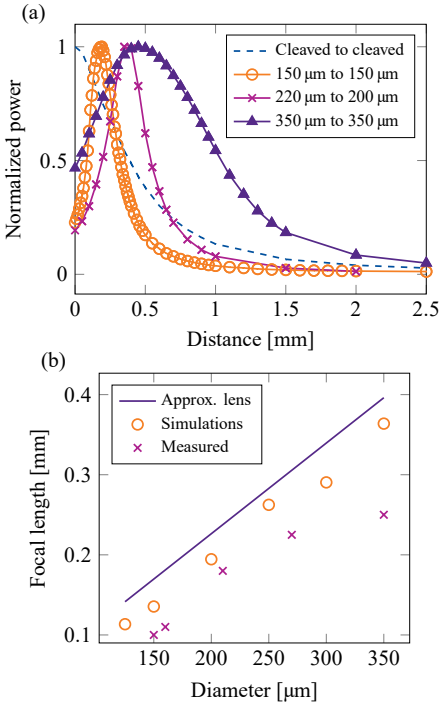

Fig. 6: Measurements and simulations of the transmission between pairs of cleaved fibers and spherical lensed fibers sized 150 µm, 210 µm and 350 µm in air. In (a), transmission measurements of the normalized power of the full spectrum. In (b), the geometric optics approximation (Eq. (5)), eigenmode simulations for the first overtone, and half the length at maximum transmittance extracted from (a).

As discussed in Section 2, the losses should be minimized and $\kappa(l)$ optimized. The absorption in air is negligible and Eq. (4) simplifies to $P_{\text{in}} = \kappa(l)P_{\text{out}}$. The focal length was determined by half of the distance at maximum transmission. The experimentally measured focal lengths are presented in Fig. 6(b) with the focal lengths predicted by the geometrical optics approximation and eigenmode simulations. In air, the eigenmode simulations give a linear, but shorter focal length than the prediction by geometrical optics in the first overtone. Imperfect alignment and imperfections introduced while melting the fiber tip could partly explain the general shorter focal length than predicted by the eigenmode simulations. The discrepancy could also come from the finite number of modes excited in the eigenmode simulation, which may over-estimate the focal length. Due to the low dispersion in air and the moderate dispersion in fused quartz ($\Delta n_a \approx 1 \times 10^{-5}$, $\Delta n_s \approx 0.01$, and $\Delta n_w \approx 0.03$ difference between 1.5 µm and 2.3 µm), this is approximately equal for the full wavelength range of interest. At a larger sphere size of 350 µm, the measured focal length appears to be slightly deviating from the linear trend. Aberrations in manufacturing could account for the deviation from linearity at larger spheres.

From a purely geometrical consideration for cleaved fibers, the transmitted power should correspond to the fraction of the area of the cone of light that hits the collecting fiber facet. The coupling between two cleaved fibers placed in close proximity should decay as a function of the distance l with a slope $-\text{NA}/2D = -1.05$, where D is the core diameter [25]. From the slope for $\kappa(l)$ for $l > 0.5$ mm of the cleaved fiber transmission in Fig. 6(a), the experimentally determined slope is approximately -1.25. Small inaccuracies in the cleave and alignment can

account for the slightly steeper slope of $\kappa(l)$ found in the experiments. When working in water, the measurements in air serve as a useful reference, as the additional absorption factor in water obscure the focusing of the lens.

The characterizing measurements were repeated in water, presented for the first overtone in Fig. 7. The strong water absorption in part of the band attenuates the beam strongly, and the focusing of the larger lenses is not as clearly visible as in air. Accurately determining the focal length in water by experiments proved challenging, but it was clear that the effective focus in water was shorter than what was expected from the simulations. The excitation of modes by a Gaussian source in the eigenmode simulations could differ significantly from the experimental light source, resulting in different propagation paths within the lens. Another mode distribution expanding faster within the lens could account for as much as a 75 % decrease in focal length. The measurements are in agreement with the asymmetry around the focal point observed by Bescherer et al. [20]. A large benefit in coupling with lensed fibers was seen. For example, the transmission at 0.4 mm could be doubled at λ = 1.6 µm by using two 150 µm lensed fibers as compared to two cleaved fibers. At longer path lengths, such as 1.5 mm, the transmission of all three fibers lensed with spheres sized 150 µm, 220 µm and 350 µm was more than doubled that of the cleaved fibers. Although a clear focus was not easily identifiable for larger sphere sizes in water, the transmission of lensed fibers with diameters 220 µm and 350 µm did not decay to zero for longer path lengths compared to the other lensed fibers and the cleaved reference. Based on the transmission in water, the path length of maximum transmission appears to occur at distances shorter than the focal length, and certainly shorter than a $2f$-system. Table 2 gives an updated summary of the corresponding lens sizes to the optimal path lengths.

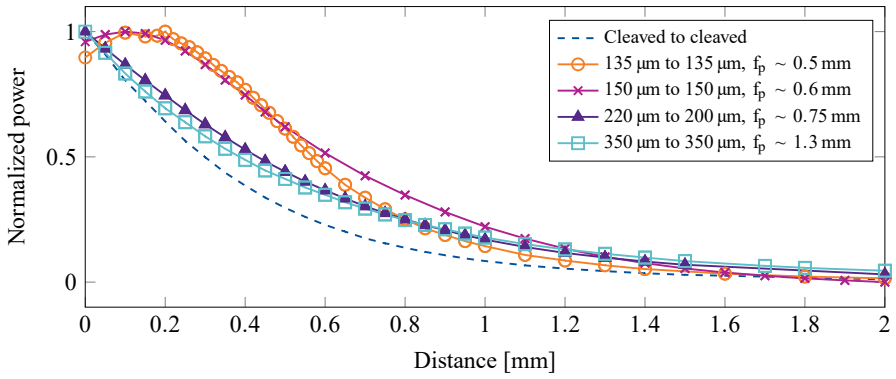

Fig. 7: The normalized coupling efficiency in transmission of aligned fibers with spherical lenses of 135 µm, 150 µm, 210 µm and 350 µm in water in the the first overtone (λ =1.5 to 1.85 µm). The predicted focal lengths (f_p) of the given sphere sizes from Fig. 5(a) are listed in the legend.

Optimal parameters	l	d
First overtone (1.6 µm)	1 to 2 mm	150 to 350 µm
Combination band (2.2 µm)	0.4 to 0.5 mm	<200 µm

Table 2: The optimal lens diameter d at the optimal l in water (as determined by [18]) for the wavelength ranges of interest from experimental measurements. For comparison with the eigenmode simulations, see Table 1.

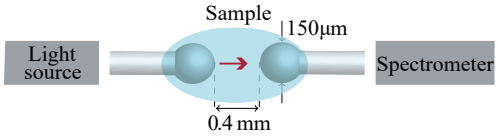

Fig. 8: The experimental setup for the sample application, aqueous glucose.

5. Measurement of aqueous glucose with NIR spectroscopy

D-(+)-Glucose powder from Sigma-Aldrich (USA) was dissolved in pure water from a RiOs 50 water purification system from Merck (Germany). 83 mM to 50 mM aqueous glucose was measured at a path length of 0.4 mm, which is the optimum path length for aqueous samples for transmission in the combination band [18]. Based on the initial measurements, a lens of 150 µm was chosen, giving high transmission in both the combination band and the first overtone. A schematic of the setup is shown in Fig. 8. The same 10 mW fiber coupled broad band source and spectrometer were used as in the experimental characterization. The fibers were aligned in a v-groove and immobilized with epoxy resin. The spectra were prepared by subtracting the dark noise background and the absorbance was found using Eq. (3). The spectra were recorded twice, with an integration time of 60 ms. A reference intensity I_0 was recorded before and after the sample set, in air. After sampling, the spectra were smoothed using Savitzky-Golay (second order, 11 smoothing points), moving average with four smoothing points, and mean centered. Multiplicative scattering correction (MSC) [26] was applied to remove baseline shifts. Fig. 9 present the resulting difference spectra with regards to water.

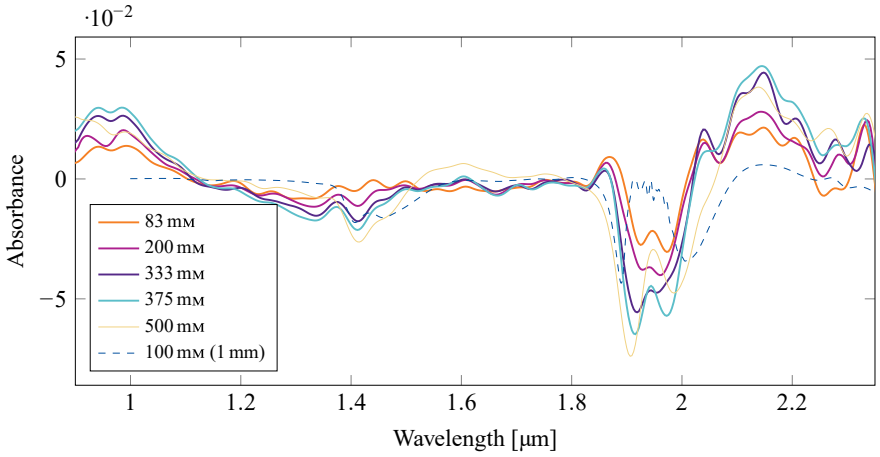

Fig. 9: Aqueous glucose measured at 0.4 mm path length with a 150 µm spherical lens. The dashed line shows a spectrum from 100 mM aqueous glucose acquired in a 1 mm path length cuvette at a commercial spectrometer system.

The spectra with a higher glucose concentration absorb more in the combination band and less in the high-absorbing water peak between 1.85 µm to 2.05 µm and the water absorption peak at 1.4 µm, illustrating the displacement factor. Although not so visible to the human eye on this figure, the glucose features in the first overtone are also detectable. The water peak at 1.85 µm to 2.1 µm and the edges of the spectra below 1.05 µm and above 2.3 µm were down-weighted as the strong absorption and/or lower detector performance at these wavelengths may lower the SNR. In addition, the high absorbance in the water peaks are easily affected by any solute, and not just glucose. These high absorbing water peaks are therefore susceptible to interferents.

A partial least squares regression (PLSR) algorithm was applied with two latent variables and cross-validation. The resulting calibration model is shown in Fig. 10, and yielded a mean absolute percentage error (MAPE) of calibration of 4.3 % and a MAPE of cross-validation of 7.8 %. The sensitivity is acceptable as a proof of principle, but requires further improvement if the setup is to be used in measuring low concentrations of glucose such as within the body.

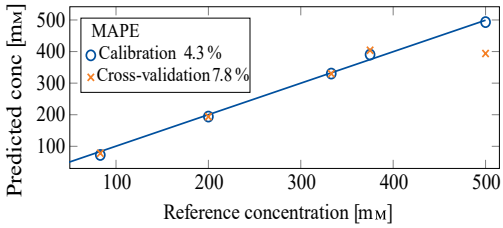

Fig. 10: Calibration model for aqueous glucose measured at 0.4 mm with 150 µm spherical lenses. The error is presented in mean absolute percentage error (MAPE).

We have also compared the obtained spectra to a 100 mM glucose spectrum acquired with a commercially available Foss (Denmark) Metrohm XDS 2000 spectrometer with a cuvette of path length 1 mm. The resulting difference spectra can be seen as the dashed line in Fig. 9. Although both the path length and the concentrations are different, some qualitative observations can be made. The signal at the combination band is stronger than for the spectrum taken using the commercial cuvette spectrometer. In the commercial cuvette spectrometer, the signal from the water absorbance peak at 1.85 µm to 2.05 µm is attenuated from the longer path length, but not in the setup presented here. The signal from the first overtone is not so clearly visible in either spectrum. The negative absorbance compared to water around 1.4 µm can be observed in all spectra. Looking at the spectra, the spherical lens setup yields more noise, probably caused by several effects. The OceanOptics NIRQuest512-2.5 spectrometer has a lower spectral resolution than the Foss Metrohm XDS 2000. The commercial cuvette spectrometer also utilizes a reference beam, while we have taken the light spectrum at the beginning of the measurements. In addition, Foss utilizes a collimated 50 W lamp, compared to 9 W from our broad band source. Although the fiber coupled effect is not known, it is likely at least an order of magnitude higher than what was used here. By increasing the effect of our source, we expect to increase the SNR considerably.

6. Discussion and conclusion

The output of lensed fiber tips of MM fibers in the NIR range has been simulated and characterized in air and water for sphere sizes in the range 125 µm to 350 µm. The lensed fibers were placed in a transmission setup, and it was shown that the length of maximum transmitted power can be tailored to the sample and the wavelength region of interest by adjusting the sphere size d.

The system of maximum $\kappa(l)$ was assumed to be the system of maximum SNR when $l = l_{\text{opt}}$, although this was not confirmed. It was also assumed that Beer-Lambert's law (Eq. (3)) holds true in the focus, i.e. that the focusing does not induce any non-linear effects. For the application of optical trapping, it has been shown that the temperature increased by absorption in a focused beam is linearly dependent on the source power in the range 0 mW to 150 mW [27]. For 10 mW source power as used here with losses in coupling from a 400 µm to a 105 mm core, the assumption likely holds. Another assumption made was that the path length has not been affected by the focusing. Using ray optics, the extreme case was estimated to a 3.3 % increase in path length, which is considered negligible.

At longer distances in water, a clear focus was not measured. From the air measurements, we have proven that the lenses have the focusing properties as expected. We believe that the effect

could partly be explained by small misalignments and imperfections in the lenses having an impact at larger fiber separations. The alignment was controlled down to 10 µm with an indicator (Mitutoyo, Japan), which limits the effect of misalignment to approximately 10 % reduction in the transmitted intensity. The measurements in Fig. 7 were repeatable also at a 6-axis fiber alignment stage (Elliot Scientific, UK) and with different lensed fibers. An attempt was made to correct the signal for the strong water absorption by dividing by the attenuation factor $\exp(-\alpha l)$, which also did not highlight any focus. Whether the effect is due to small inaccuracies in manufacturing, misalignment or another phenomena, it was measured consistently and should be taken into account in design.

In general, the measurements show consistently higher losses than the geometrical optics approximation and the eigenmode simulations. In the approximations and the simulations, scattering at the surfaces was ignored and the refractive index of the lenses was assumed to be uniform. A Gaussian source was used in the eigenmode simulations. However, the broad band source may be more similar to a Lambertian source as used in simulations by Bescherer et al. [20]. The resulting simulated coupling efficiencies they present correspond with the shape of the coupling efficiency curves measured here. The discrepancy in simulated and experimental results can largely be explained by the different propagation paths in the lens if the broad band light source differed greatly from a Gaussian source. In addition, the 20 µm of cladding in the fiber may have led to refraction within the lens and altered focusing properties of the lenses as compared to the simulations that would show itself experimentally as higher coupling efficiencies at short distances. The scattering from the back of the larger sphere shown in Fig. 2(b) could be caused by back-reflected rays, whispering gallery modes within the sphere, or other effects induced by stress in manufacturing larger lenses. Although the arc procedure generating the lenses was fairly reproducible, slight changes in the cleave could influence the results.

In the sample application of glucose measurements, the fiber-based transmission setup compares well in SNR to a commercial cuvette spectrometer and excels in ease of use, flexibility and adaptability. The commercial cuvette spectrometer has the advantage of a more stable and smoother signal indicating that our spectrometer setup can be improved by further optimization of the immobilization, source power and possibly the signal processing. In regards to the ability to sense glucose, the chosen range is well above the normal physiological range (4 mM to 8 mM). The precision of commercial continuous glucose monitoring devices normally has a MAPE of 15 % to 20 % [3]. However, due to the different range, this is not directly comparable to the MAPE of cross-validation of 7.8 % obtained here. The SNR must be high enough to distinguish differences in intensity on the order of 1×10^{-3} % corresponding to a change of 1 mM. These preliminary results are noteworthy on account of applying optical fiber-design to meet the needs of NIR spectroscopy, a widely used and diverse technique. The experimental characterization of lensed MM fibers with diameters 125 µm to 350 µm supplements previously reported work in the field [20] that can be utilized beyond NIR spectroscopy.

In future work, a transflectance probe will be manufactured by placing the fibers in parallel facing a mirror. Such a miniaturized probe can enable flexible measurements of liquids that are not extractable or in remote locations, for example in the continuous monitoring of glucose levels in diabetic patients by measuring the peritoneal fluid [7].

Acknowledgements Thanks to Nofima (Norway) and Bjørg Ådahl for help with and use of the Foss Spectrometer. We would also like to thank Harald Martens for valuable input on the signal processing.

Funding Silje S. Fuglerud is funded by the Central Norway Regional Health Authority, project number 46055510. The project is part of the Double Intra-peritoneal Artificial Pancreas project, project number 248872, funded by the Research Council of Norway.

References and links

1. NCD Risk Factor Collaboration, "Worldwide trends in diabetes since 1980: a pooled analysis of 751 population-based studies with 4.4 million participants," The Lancet **387**, 1513 – 1530 (2016).
2. E. Ryckeboer, R. Bockstaele, M. Vanslembrouck, and R. Baets, "Glucose sensing by waveguide-based absorption spectroscopy on a silicon chip," Biomed. Opt. Express **5**, 1636–1648 (2014).
3. I. L. Jernelv, K. B. Milenko, S. S. Fuglerud, D. R. Hjelme, R. Ellingsen, and A. Aksnes, "A review of optical methods for continuous glucose monitoring," Appl. Spectrosc. Rev. DOI:10.1080/05704928.2018.1486324 (posted 15 November 2018, in press).
4. M. Goodarzi, S. Sharma, H. Ramon, and W. Saeys, "Multivariate calibration of nir spectroscopic sensors for continuous glucose monitoring," TrAC Trends Anal. Chem. **67**, 147 – 158 (2015).
5. Y. Y. Katsuhiko Maruo, "Near-infrared noninvasive blood glucose prediction without using multivariate analyses: introduction of imaginary spectra due to scattering change in the skin," J. Biomed. Opt. **20**, 047003 (2015).
6. S. Sharma, M. Goodarzi, J. Delanghe, H. Ramon, and W. Saeys, "Using experimental data designs and multivariate modeling to assess the effect of glycated serum protein concentration on glucose prediction from near-infrared spectra of human serum," Appl. Spectrosc. **68**, 398–405 (2014).
7. A. L. Fougner, K. Kölle, N. K. Skjærvold, N.-A. L. Elvemo, D. R. Hjelme, R. Ellingsen, S. M. Carlsen, and Ø. Stavdahl, "Intraperitoneal glucose sensing is sometimes surprisingly rapid," Model. Identif. Control. **37**, 121 – 131 (2016).
8. H. Lee, W. Yue, and S. Lee, "Design of an alignment tolerant miniature optical subassembly module," IEEE Photonics J. **6**, 1–9 (2014).
9. G. J. Kong, J. Kim, H. Y. Choi, J. E. Im, B. H. Park, U. C. Paek, and B. H. Lee, "Lensed photonic crystal fiber obtained by use of an arc discharge," Opt. Lett. **31**, 894–896 (2006).
10. G. Rego, "Fibre optic devices produced by arc discharges," J. Opt. **12**, 113002 (2010).
11. S. Y. Ryu, H. Y. Choi, J. Na, W. J. Choi, and B. H. Lee, "Lensed fiber probes designed as an alternative to bulk probes in optical coherence tomography," Appl. Opt. **47**, 1510–1516 (2008).
12. A. L. Barron, A. K. Kar, and H. T. Bookey, "Dual-beam interference from a lensed multicore fiber and its application to optical trapping," Opt. Express **20**, 23156–23161 (2012).
13. J. Mo, W. Zheng, and Z. Huang, "Fiber-optic raman probe couples ball lens for depth-selected raman measurements of epithelial tissue," Biomed. Opt. Express **1**, 17–30 (2010).
14. H. Y. Choi, S. Y. Ryu, J. Y. Kim, G. H. Kim, S. J. Park, B. H. Lee, and K. S. Chang, "Microlensed dual-fiber probe for depth-resolved fluorescence measurements," Opt. Express **19**, 14172–14181 (2011).
15. H.-P. Loock, "Ring-down absorption spectroscopy for analytical microdevices," TrAC Trends Anal. Chem. **25**, 655 – 664 (2006). On-site Instrumentation and Analysis.
16. J. T. Olesberg, L. Liu, V. V. Zee, and M. A. Arnold, "In vivo near-infrared spectroscopy of rat skin tissue with varying blood glucose levels," Anal. Chem. **78**, 215–223 (2006).
17. S. W. Harun, A. A. Jasim, H. A. Rahman, M. Z. Muhammad, and H. Ahmad, "Micro-ball lensed fiber-based glucose sensor," IEEE Sensors J. **13**, 348–350 (2013).
18. P. S. Jensen and J. Bak, "Near-infrared transmission spectroscopy of aqueous solutions: Influence of optical pathlength on signal-to-noise ratio," Appl. Spectrosc. **56**, 1600–1606 (2002).
19. M. Goodarzi and W. Saeys, "Selection of the most informative near infrared spectroscopy wavebands for continuous glucose monitoring in human serum," Talanta **146**, 155 – 165 (2016).
20. K. Bescherer, D. Munzke, O. Reich, and H.-P. Loock, "Fabrication and modeling of multimode fiber lenses," Appl. Opt. **52**, B40–B45 (2013).
21. F. Träger, *Springer Handbook of Lasers and Optics* (Springer, New York, NY, 2007), pp. 53–54.
22. I. H. Malitson, "Interspecimen comparison of the refractive index of fused silica," J. Opt. Soc. Am. **55**, 1205–1209 (1965).
23. G. M. Hale and M. R. Querry, "Optical constants of water in the 200-nm to 200-μm wavelength region," Appl. Opt. **12**, 555–563 (1973).
24. L. Kou, D. Labrie, and P. Chylek, "Refractive indices of water and ice in the 0.65- to 2.5-μm spectral range," Appl. Opt. **32**, 3531–3540 (1993).
25. H. Tsuchiya, H. Nakagome, N. Shimizu, and S. Ohara, "Double eccentric connectors for optical fibers," Appl. Opt. **16**, 1323–1331 (1977).
26. A. Kohler, M. Zimonja, V. Segtnan, and H. Martens, "Standard normal variate, multiplicative signal correction and extended multiplicative signal correction preprocessing in biospectroscopy," in *Comprehensive Chemometrics,* S. D. Brown, R. Tauler, and B. Walczak, eds. (Elsevier, 2009), pp. 139–162, 2nd ed.
27. E. J. G. Peterman, F. Gites, and C. F. Schmidt, "Laser-induced heating in optical traps," Biophys. J. **84**, 1308–1316 (2003).